Research Square

Preprints are preliminary reports that have not undergone peer review.
They should not be considered conclusive, used to inform clinical practice,
or referenced by the media as validated information.

DTI-based mesoscale connectomics detects survival-relevant white matter substructures in glioblastoma patients

Andreas Stadlbauer

andi@nmr.at

Karl Landsteiner University of Health Sciences

Stefan Oberndorfer

Karl Landsteiner University of Health Sciences

Gertraud Heinz

Karl Landsteiner University of Health Sciences

Arnd Dörfler

Friedrich-Alexander-Universität Erlangen-Nürnberg

Franz Marhold

Karl Landsteiner University of Health Sciences

Oliver Schnell

Friedrich-Alexander-Universität Erlangen-Nürnberg

Mario Dorostkar

Karl Landsteiner University of Health Sciences

Uwe Meyer-Bäse

Florida State University

Anke Meyer-Bäse

Florida State University

Research Article

Keywords: Connectomics, glioblastoma, survival analysis, correlational tractography, diffusion tensor imaging

Posted Date: September 3rd, 2026

DOI: https://doi.org/10.21203/rs.3.rs-10392049/v1

License: This work is licensed under a Creative Commons Attribution 4.0 International License.
Read Full License

Additional Declarations: No competing interests reported.

Abstract

Purpose.

Glioblastoma (GB) is a highly invasive and lethal primary brain tumor, with survival affected by tumor location, clinical factors, and molecular features. White matter (WM) tracts serve as pathways for GB cell migration, but the effects of microstructural integrity within specific fiber subcomponents on overall survival (OS) remain unclear. This study aimed to determine whether correlational tractography can identify WM tract segments whose microstructural integrity correlates with OS in GB patients.

Methods.

Diffusion tensor imaging and clinical data from 498 GB patients in the UPENN-database were analyzed. Connectometry and correlational tractography reconstructed WM tracts and identified subcomponents whose fractional anisotropy (FA) correlated with OS, controlling for age, sex, and extent of resection. Kaplan-Meier and Cox-proportional-hazards models assessed survival differences based on FA.

Results.

Normal FA in reconstructed fiber subcomponents was significantly associated with longer OS across the whole brain (median OS 487 vs. 207 days) and in left- (488 vs. 241 days) and right-hemispheric tumors (493 vs. 216 days). Subclusters of the thalamic radiation and corpus callosum were the major tracts correlating with OS. Lobe-specific patterns reflected normative anatomy: projection fibers predominated in central tumors, commissural fibers in frontal tumors, and association fibers in temporal tumors. Cox models confirmed FA was independently associated with reduced hazard across the whole brain (HR = 0.555) and in both hemispheres (HR = 0.589).

Conclusion.

Connectometry and correlational tractography identify WM subcomponents whose microstructural integrity is closely linked to survival in GB, highlighting their potential value as biomarkers for future prognostic modeling.

Introduction

Glioblastoma (GB) remains among the most aggressive and intractable primary brain tumors in adults. A hallmark of the disease is its diffusely infiltrative nature, with tumor cells migrating away from the core lesion into adjacent and even distant brain regions, making accurate delineation of tumor margins and thus complete surgical removal almost impossible. Despite advances in neurosurgery, neuroimaging, and adjuvant therapies, patient outcomes remain dismal with a median overall survival of 12–18 months

[1]. Long-term survival is exceedingly rare: less than 7% of patients survive beyond five years, and one-year survival rates hover around 40%, declining to 17% at two years [2]. Key factors known to influence survival include the extent of resection (EOR) achieved during surgery, patient age, and the genetic and molecular profile of the tumor [3].

In vivo experiments, histological examinations, and imaging studies have shown that GB cells preferentially align with axonal bundles, using the anisotropic architecture of white matter (WM) tracts as channels for migration, i.e., GB cells tend to follow the predominant fiber orientation [4–6]. The integrity of these affected pathways is gradually compromised and ultimately destroyed. This highly infiltrative behavior of GB cells is a major reason for treatment failure, rapid tumor recurrence, and poor prognosis [7]. For example, infiltration of critical midline structures such as the corpus callosum is associated with a significantly lower median survival time, in some cases as short as 6–9 months [8].

Connectomics is a field of neuroscience dedicated to mapping and analyzing complex neural networks through computational modeling of imaging data, emphasizing the intricate topology of neural connectivity and its functional implications beyond traditional anatomical frameworks [9]. Recent connectomics and neuroimaging research has demonstrated that glioblastoma cell infiltration follows non-random patterns aligned with underlying brain connectivity, supporting the notion that a network-based framework is crucial for understanding, mapping, and ultimately managing tumor invasion [10, 11].

Connectomics can be subdivided into micro-, meso-, and macroscale approaches, each representing a specific level of neural organization. Microscale connectomics examines neuronal and synaptic connectivity, primarily using histological and electron-microscopic methods, which are unsuitable for in vivo studies in humans. Macroscale connectomics investigates large-scale structural and functional brain networks, such as interhemispheric connections and major WM tracts, using imaging techniques like diffusion magnetic resonance imaging (MRI) and tractography to quantify connection strengths between cortical or subcortical parcels and to derive network graphs [12]. Mesoscale connectomics bridges the micro- and macroscale, linking the connectivity of neuronal populations with the large-scale architecture of brain networks by mapping small assemblies of neurons and examining how these intermediate structures support communication and integration across the brain. In GB, mesoscale connectomics is particularly valuable because it can localize subtle, spatially confined alterations in microstructural integrity along WM tracts, potentially identifying zones of tumor invasion that deviate from normative connectivity patterns [13].

Diffusion tensor imaging (DTI) and its advanced variants are the primary neuroimaging techniques used for three-dimensional reconstruction of WM fiber tracts by modeling the anisotropic diffusion of water molecules. Connectometry [14] is a mesoscale connectomics method that uses a statistical framework to relate local microstructural metrics derived from DTI data, such as spin distribution functions or fiber density, to variables of interest in the subjects. This approach enables the identification of fiber segments and subcomponents whose local connectome properties correlate with the variable of

interest. Correlational tractography [15], closely linked to connectometry, leverages group-wise correlations of connectometry data to map statistical associations between structural connectivity patterns and clinical or behavioral measures. Unlike traditional tractography, this approach identifies affected tracts by their functional or clinical relevance, enabling the detection of subtle structural changes associated with pathophysiology [14, 15]. Partial correlations between DTI metrics (e.g., fractional anisotropy) and a study variable (e.g., survival) are first calculated while controlling for covariates like age or sex. Then, t-statistics from these correlations across voxels seed deterministic fiber tracking to generate fiber tracts whose microstructural properties systematically correlate with the variable of interest, resulting in a refined map of fiber segments associated with the measure of interest across subjects. Connectometry and correlational tractography have been applied to investigate associations between white matter tract integrity and clinical questions in neurological, behavioral, or neuropsychiatric conditions [16].

We hypothesized that connectometry and correlational tractography identify WM tract segments whose microstructural integrity is associated with overall survival in patients with glioblastoma. By analyzing tract segments rather than whole-tract averages, this approach may detect subtle perturbations in microstructural integrity, thereby creating a refined map of fiber subcomponents associated with survival. To test this, we analyzed DTI and survival data from 498 patients in The Cancer Imaging Archive using connectometry combined with correlational tractography.

Materials and Methods

Patient Population

This retrospective study was approved by the Institutional Review Boards of the Lower Austrian Provincial Government and the Friedrich-Alexander University (FAU) Erlangen-Nürnberg. The study was performed in accordance with the ethical standards as laid down in the 1964 Declaration of Helsinki and its later amendments. We used a publicly available database from The Cancer Imaging Archive (TCIA; https://www.cancerimagingarchive.net/collection/upenn-gbm) that included 630 patients with glioblastoma from the UPenn-GBM cohort [17] who had given their consent to data collection in this earlier study. All included patients were histologically diagnosed with glioblastoma isocitrate dehydrogenase (IDH) wildtype. Incomplete information on IDH gene status led to patient exclusion according to the 2021 WHO criteria [17]. Patients with missing overall survival (OS) data were also excluded from the study, there were no censored observations. Ultimately, 498 patients (199 females, 299 males, mean age ± standard deviation 63.4 ± 11.8 years, age range 21–89 years) were included with a median OS (mOS) of 387 days (OS range 3–2951 days).

DTI Data Acquisition and Preprocessing

From each patient included in the study, the DTI data of the pre-treatment clinical MRI scan was used in their publicly available form. Detailed information on the acquisition parameters of the DTI data can be found in previous publications [17]. In short, a DTI diffusion scheme was used, and a total of 30 diffusion sampling directions were acquired. The b-value was 1000 s/mm². The in-plane resolution was 1.72 x 1.72 mm^2. The slice thickness was 3 mm and the number of slices was 40 without gap between slices.

The preprocessing of the DTI data was carried out using the open-source software platform DSI Studio (Hou "" version; http://dsi-studio.labsolver.org) [18]. Raw DTI data were converted from DICOM to SRC format, followed by a quality control procedure in the DSI Studio and resampling to an isotropic resolution of 2 mm^3. Figure 1 shows the flowchart of the four steps for pre- and postprocessing of the DTI data.

In the first step, the DTI data underwent spatial normalization through reconstruction in Montreal Neurological Institute (MNI) space using the dedicated q-space diffeomorphic reconstruction (QSDR) technique and the ICBM152 standard brain template [19]. The dispersion data from each participant was reassembled in a universal stereotaxic space, which maintains the conservation of diffusion spins after a nonlinear spatial transformation. The R^2-values of all normalized files were checked using a threshold of 0.70 to ensure that each dataset was adequately registered to the template. QSDR can be applied to DTI data to calculate the spin distribution function (SDF), as previously described [19]. The SDF provides information about the amount or density of diffusing water in any direction within a single voxel [20, 21], thereby characterizing the directional distribution of water diffusion (indicative of underlying fiber orientations) as well as the overall density of diffusing spins when integrated across all directions.

Connectometry and Correlational Tractography

In the second step, the SDFs were sampled along a dense set of local fiber directions from a common atlas (HCP-842 atlas) [22] containing 550,000 fiber trajectories to estimate the local connectome as the result of the mesoscale connectomics method called connectometry [14]. The term “local connectome” refers to the degree of connectivity in the mesoscale region of adjacent DTI data voxels within a WM bundle, defined by the density of diffusing spins. These local connectome vectors of each patient were then assembled into the local connectome matrix, where each row of the matrix represented the local connectome of a subject, and each column corresponded to each local fiber direction in the HCP-842 atlas. SDFs and local connectome values were computed for all voxels of the entire diffusion dataset, without explicit exclusion of tumor tissue, which was inherent to the connectometry framework. However, tumor cores typically show low anisotropy, disrupted diffusion directions, and a lack of coherent fiber architecture, factors that impair correlative tractography (Fig. 2).

In the third step, this local connectome matrix was associated with OS and adjusted for the factors age, gender, and extent of resection (EOR). The nonparametric Spearman method was used to derive the correlation, and the effect of the covariates was removed using a multiple regression model. The statistical significance of the correlation was checked using a permutation test [14]. The resulting t-

statistics were converted into a statistical map in local connectome space. This procedure identified local connectome regions significantly associated with OS. This statistical map then served as a seeding field for the deterministic fiber tracking in the last step.

Finally, fiber segments whose local connectome metrics showed a strong association with OS (while controlling for age, sex, and EOR) were tracked, yielding continuous segments identified through correlational tractography [15]. A deterministic fiber tracking algorithm [23] was applied using a t-score threshold of 4.2–5.2 to achieve an effect size of ≥ 0.3, corresponding to medium to strong association. To increase the specificity, the obtained tracts were further filtered by topology-informed pruning with 16 iterations [24]. A tract length threshold of 20 voxels and a false discovery rate (FDR) threshold of 0.01 was applied to select tracts. To estimate the FDR, 4000 randomized permutations of group labels were used to generate the null distribution of the tract lengths. Permutation testing enabled correction for Type-I error inflation due to multiple comparisons. The FDR, calculated as the ratio of total findings and false positives, was used to reject null hypotheses and identify tracts with significant FDR [14]. This direct estimation provided a more intuitive measure of significance. The default reconstruction settings implemented in DSI Studio were used. The number of topology-informed pruning iterations was selected based on the recommended standard settings of the software pipeline to reduce false-positive connections while preserving biologically plausible fiber trajectories.

Connectometry followed by correlation tractography was performed for the entire cohort of 498 patients, as well as for subcohorts grouped by tumor location: two subgroups with tumor location predominantly in the left or right hemisphere, and ten subgroups with tumor locations predominantly in the frontal, parietal, occipital, or temporal lobes, or in the central (basal ganglia) region of the left and right hemispheres. Tumor location (predominant hemisphere and specific lobe or central region) was determined through expert neuroradiological evaluation of contrast-enhanced T1-weighted MRI scans. The assessment was performed by consensus between an experienced neurosurgeon and a neuroradiologist, both with extensive expertise in brain tumor imaging.

Tract Analysis and Statistical Methods

Reconstructed tracts showing a significant and highly specific correlation with OS were segmented into fascicle subcomponents using the ”Recognize and Cluster” method based on a dedicated tractography atlas as part of the DSI Studio software package [18, 22]. For further analysis, the mean fractional anisotropy (FA) values of individual tract subclusters and their merged counterparts were extracted for all patients.

Statistical analyses were performed using JASP (version 0.95.2; JASP Team, University of Amsterdam) [25], an open-source graphical interface built on the R statistical environment (version 4.5.1) [26]. Normality of numeric data was assessed using the Shapiro–Wilk test, and equality of variances was evaluated with Levene’s test. Differences in mean patient age were examined via independent-samples t-test. Since overall survival times violated normality assumptions, their distributions were compared

using the Mann-Whitney *U* test. Group differences in categorical variables, such as sex and extent of resection (EOR), were assessed with the Chi-square test. All analyses were conducted with a significance threshold of $p < 0.05$.

Kaplan–Meier survival curves [27] were generated according to FA category and compared using the log-rank test. Survival differences according to age, sex, and EOR were analyzed separately. FA values were dichotomized using two approaches: (i) mean FA values derived from healthy controls, and (ii) cut-off values defined by the maximally selected rank statistics (maxstat) function from the R package survminer [28]. Normal FA values were obtained from the Stark Cross-Sectional Aging database (RRID:SCR_014171; https://www.nitrc.org/projects/stark_aging), selected for its similar DTI acquisition parameters. After normalization of the DTI data from 118 healthy volunteers using the QSDR method and import of the patients' fiber subclusters, we computed median, mean, and standard deviation for these fiber subclusters in controls. The threshold for Kaplan–Meier analysis was set at the median minus one standard deviation (approximately the 16th percentile), with FA values below this threshold considered indicative of tumor-related impairment of fiber structure. Cut-off values obtained from the two methods (controls and survminer) showed close agreement, differing only at the second decimal place. Therefore, the mean of both values was used as the optimized cut-off for Kaplan–Meier analysis. However, these cut-off values should be considered exploratory and hypothesis-generating, requiring validation in independent cohorts before potential prognostic implementation.

Cox proportional hazards models were employed to evaluate the prognostic impact of multiple variables including FA value, age, sex, and EOR, with hazard ratios (HRs) and 95% confidence intervals (CIs) calculated. Additionally, linear and exponential regression analyses were performed to assess the correlation between OS and the mean FA values of the fiber tracts. To determine whether a linear or exponential function provided the better fit, a non-nested model comparison was conducted using the Akaike Information Criterion (AIC), with lower AIC values indicating a better balance between model fit and complexity.

Results

Patient Characteristics

Demographic information (age, sex) and clinical data (EOR, OS) for the 498 glioblastoma patients from the UPenn-GBM database included in this study are summarized in **Supplementary Results** (**Table S1**). Patient subgroups are presented according to tumor location: 280 patients had tumors predominantly located in the left hemisphere and 218 in the right hemisphere. OS data are reported as median survival times with the 95% confidence intervals (CIs) in square brackets followed by range. Median OS did not differ significantly between patients with tumors in the left versus right hemisphere (Mann–Whitney U = 28,389, p = 0.181). There were also no significant differences in sex (χ^2 = 3.325, p = 0.068) or EOR (χ^2 = 2.29×10^{-4}, p = 0.988) between these subgroups.

Connectometry and Correlational Tractography versus OS

Connectometry and correlational tractography identified tract substructures in which higher FA values were associated with longer OS, i.e., significant positive correlations (FDR ≤ 0.01). No tracts showed a significant association between higher FA and shorter OS (negative correlation). The left and middle panels of Fig. 1A display the results of correlational tractography for the entire cohort of all 498 patients, encompassing all tumor localizations across the whole brain.

The major WM pathways and their subclusters that correlated with OS for glioblastoma located across the whole brain, as well as separately for tumors in the left and right hemispheres, are summarized in Table 1. For tumor locations throughout the brain, the largest proportion of pathways correlating with OS involved the basal ganglia projection system (73.9%), with the anterior and superior thalamic radiation comprising the largest subclusters. Commissural tracts, primarily the corpus callosum, accounted for 15.7% of the total fiber volume, while association tracts (cingulate, 9.0%) and projection tracts to the brainstem (non-decussating dentato-rubro-thalamic tract, ndDRTT, 1.4%) made up smaller proportions. The left and middle panels of Figs. 1B and **C** illustrate the subclusters of the basal ganglia projection tracts and corpus callosum, respectively, which were identified through tract recognition followed by clustering.

Table 1
Major white matter pathways and their Subclusters that correlated with OS for glioblastoma locations in the whole brain and left- and right-hemispheric tumors.

Tumor Loc.	Major WM pathway	%	Subclusters	%
Whole Brain	Projection, Basal Ganglia	73.9	Thalamic Radiation, Anterior, right	25.6
			Thalamic Radiation Superior, left	16.9
			Fornix, left	16.7
			Thalamic Radiation, Anterior, left	11.5
			Thalamic Radiation Superior, right	3.2
	Projection, Brainstem	1.4	Non-decussating Dentato-Rubro-Thalamic Tract, left	1.4
	Commissure	15.7	Corpus Callosum, Body	11.3
			Corpus Callosum, Tapetum	2.4
			Corpus Callosum, Forceps Major	2.0
	Association	9.0	Cingulum, Frontal-Parahippocampal, left	9.0
Left Hemisphere	Projection, Basal Ganglia	54.6	Fornix, left	31.6
			Thalamic Radiation Superior, left	16.9
			Thalamic Radiation, Anterior, left	6.1
	Projection, Brainstem	2.8	Non-decussating Dentato-Rubro-Thalamic Tract, left	2.8
	Commissure	36.1	Corpus Callosum, Body	34.0
			Corpus Callosum, Tapetum	2.0
	Association	6.5	Cingulum, Frontal-Parahippocampal, left	6.5
Right Hemisphere	Projection, Basal Ganglia	57.6	Thalamic Radiation, Anterior, right	45.2
			Fornix, right	8.8
			Thalamic Radiation Superior, right	3.6
	Commissure	42.4	Corpus Callosum, Forceps Minor	23.8
			Corpus Callosum, Body	10.2

Percentage values indicate the proportion of the reconstructed total fiber volume that correlated with OS.

Tumor Loc.	Major WM pathway	%	Subclusters	%
			Corpus Callosum, Forceps Major	8.4
Percentage values indicate the proportion of the reconstructed total fiber volume that correlated with OS.				

Both left- and right-hemispheric glioblastomas exhibited a similar pattern. The total volume of fiber structures correlating with OS was dominated by the basal ganglia projection tracts (fornix and thalamic radiations), accounting for 54.6% in left-hemispheric and 57.6% in right-hemispheric glioblastomas. This was followed by the corpus callosum, contributing 36.1% and 42.4% in left- and right-hemispheric cases, respectively (Table 1). The left panels of Figs. 2A and **B** show the overall correlational tractography results for left- and right-hemispheric glioblastomas, respectively, while Figs. 2C and **D** display the corresponding subclusters for the projection tracts, and Figs. 2E and **F** show the subclusters in the corpus callosum.

For tumor localizations by brain lobes, a more specific but expected pattern emerged: the WM pathways that predominated were those constituting the major fiber systems of the respective lobes in the normal brain (**Supplementary Results, Table S2**).

For glioblastoma located in central regions, projection fibers (mainly the thalamic radiation; > 98%) correlated with OS. In frontal tumors, commissural pathways (mainly the corpus callosum; >95%), were dominant, whereas in temporal tumors, association fibers, particularly the inferior fronto-occipital fasciculus and inferior longitudinal fasciculus, comprised the majority (> 88%). Finally, glioblastomas located in the occipital and parietal lobes exhibited a more heterogeneous pattern, with projection (16–39%), commissural (15–51%), and association fibers (26–69%) contributing to the correlations with OS.

Survival and Hazards

Kaplan-Meier analyses revealed significant differences in OS between patient subgroups with mean FA values within the normal range and those with decreased mean FA values in the reconstructed fiber tracts. For the entire cohort, encompassing all tumor localizations across the brain, patients with normal FA value in the fiber tracts identified by connectometry and correlational fiber tractography had a significantly longer median OS (mOS) of 487 days (95% CI, 445–528 days) compared to 207 days (186–282 days) in patients with decreased FA values (log-rank test $\chi^2 = 62.77$; $p < 0.001$). The one-year survival rate was more than twice as high in patients with normal mean FA values in relevant fiber tracts compared to those with reduced FA (68.7% vs. 32.8%). The two- and three-year survival rates were approximately tenfold higher in the normal FA group (27.6% vs. 2.1% and 15.3% vs. 1.4%, respectively; Table 2). The rightmost panel of Fig. 1A shows the corresponding Kaplan–Meier plot, while the adjacent four panels illustrate the associated fiber tracts from different viewing angles. Separate Kaplan-Meier analyses for subclusters in the projection tracts and corpus callosum (Figs. 1B **and C**) revealed that

reduced FA in both subclusters similarly negatively impacted OS, with a somewhat stronger effect observed in the projection subcluster.

Table 2
Kaplan-Meier Survival Analyses.

Tumor Loc.	FA	mOS [CI]	1a - Surv.	2a-Surv.	3a-Surv.	Log-rank p (χ^2)
Whole Brain	decr.	207 [186, 282]	32.8	2.1	1.4	–
(N = 498)	norm.	487 [445, 528]	68.7	27.6	15.3	< 0.001 (62.77)**
Left Hemisphere	decr.	241 [185, 343]	38.8	11.8	4.6	–
(N = 280)	norm.	488 [434, 565]	71.1	25.8	12.5	< 0.001 (22.67)**
Right Hemisphere	decr.	216 [154, 355]	34.8	5.8	2.9	–
(N = 218)	norm.	493 [435, 590]	63.8	31.5	19.5	< 0.001 (34.79)**
Left Central	decr.	138 [99, 427]	26.3	10.5	5.3	–
(N = 28)	norm.	416 [338, NR]	66.7	22.2	NR	0.267 (1.23)
Left Frontal	decr.	170 [85, 324]	25.0	10.7	3.6	–
(N = 67)	norm.	419 [364, 613]	61.5	23.1	12.8	0.003 (8.82)*
Left Occipital	decr.	393 [234, 578]	52.6	15.8	15.8	–
(N = 45)	norm.	561 [440, 765]	76.9	30.8	19.2	0.068 (3.32)
Left Parietal	decr.	374 [257, 445]	60.0	4.0	NR	–
(N = 67)	norm.	411 [346, 533]	54.8	21.4	11.9	0.060 (3.55)
Left Temporal	decr.	376 [193, 551]	51.7	21.7	5.0	–
(N = 73)	norm.	454 [320, NR]	69.2	7.4	NR	0.493 (0.47)

FA = fractional anisotropy, decr. = decreased FA values, norm. = normal FA values, mOS = median OS, CI = 95% confidence interval of mOS, 1a-Suv. = 1-year survival rate, 2a-Suv. = 2-year survival rate, 3a-Suv. = 3-year survival rate, NR = not reached. *Statistically significant for $p < 0.05$; **Statistically significant for $p < 0.001$.

Tumor Loc.	FA	mOS [CI]	1a - Surv.	2a-Surv.	3a-Surv.	Log-rank p (χ^2)
Right Central	decr.	143 [61, 385]	14.3	NR	NR	–
(N = 33)	norm.	464 [355, 1055]	63.2	31.6	15.8	< 0.001 (11.37)**
Right Frontal	decr.	295 [200, 490]	46.4	14.3	14.3	–
(N = 48)	norm.	455 [390, 781]	80.0	25.0	10.0	0.315 (1.01)
Right Occipital	decr.	270 [166, 561]	28.6	NR	NR	–
(N = 32)	norm.	623 [430, 1159]	72.2	33.3	27.8	< 0.001 (11.76)**
Right Parietal	decr.	273 [153, 505]	39.3	10.7	7.1	–
(N = 43)	norm.	684 [411, 925]	80.0	40.0	13.3	0.011 (6.39)*
Right Temporal	decr.	381 [195, 626]	51.5	24.2	21.1	–
(N = 62)	norm.	693 [443, 960]	65.5	44.8	20.7	0.597 (0.28)

FA = fractional anisotropy, decr. = decreased FA values, norm. = normal FA values, mOS = median OS, CI = 95% confidence interval of mOS, 1a-Suv. = 1-year survival rate, 2a-Suv. = 2-year survival rate, 3a-Suv. = 3-year survival rate, NR = not reached. *Statistically significant for $p < 0.05$; **Statistically significant for $p < 0.001$.

In left- and right-hemispheric glioblastomas, reduced FA in reconstructed fiber bundles similarly affected OS, though the effect was somewhat stronger in right-hemispheric tumors. This effect was particularly evident in the differences observed in the two- and three-year survival rates (Table 2). The Kaplan-Meier curves for the predominantly left-hemispheric glioblastomas, along with the corresponding reconstructed fiber structures, are shown in Fig. 2A, while the plots for right-hemispheric glioblastomas are shown in Fig. 2B. Figures 2C and **E** and Figs. 2D and **F** present Kaplan-Meier analyses separately for subclusters in the projection pathways and the corpus callosum, with their corresponding fiber structures. No major differences were observed in survival curves between these subclusters. When examining survival curves by tumor location in cerebral lobes, all subgroups exhibited decreased mOS and reduced survival rates associated with decreased FA in the relevant fiber structures. However, statistically significant differences were observed only for tumors located in the left frontal lobe, as well as the right central region, and the right occipital and parietal lobes (Table 2).

According to the Cox proportional hazards models (Table 3), across the whole brain, an increase in FA (ΔFA = 0.1) was significantly associated with improved survival and a reduced hazard ratio (HR 0.555, 95% CI: 0.467–0.658; $p < 0.001$). Increasing age was independently associated with poorer survival (HR 1.017 per year, 95% CI: 1.009–1.025; $p < 0.001$). Similar results were observed for left-hemispheric glioblastomas (FA HR = 0.589, 95% CI: 0.471–0.737; age HR = 1.011, 95% CI: 1.001–1.022) and right-hemispheric glioblastomas (FA HR = 0.589, 95% CI: 0.480–0.724; age HR = 1.027, 95% CI: 1.014–1.040).

Table 3
Cox proportional hazards regression.

Tumor Loc.	FA	Age	Gender (M)	EOR (> 90%)
Whole Brain	0.555 [0.467, 0.658]	1.017 [1.009, 1.025]	0.920 [0.679, 1.249]	0.788 [0.586, 1.060]
(N = 498)	< 0.001**	< 0.001**	0.594	0.115
Left Hemisphere	0.589 [0.471, 0.737]	1.011 [1.001, 1.022]	1.018 [0.661, 1.568]	0.802 [0.529, 1.216]
(N = 280)	< 0.001**	0.032*	0.936	0.299
Right Hemisphere	0.589 [0.480, 0.724]	1.027 [1.014, 1.040]	0.769 [0.487, 1.214]	0.800 [0.521, 1.227]
(N = 218)	< 0.001**	< 0.001**	0.259	0.306
Left Central	0.461 [0.256, 0.829]	1.032 [0.986, 1.080]	1.366 [0.356, 5.246]	0.706 [0.112, 4.437]
(N = 28)	0.010*	0.176	0.649	0.710
Left Frontal	0.666 [0.498, 0.890]	1.017 [0.998, 1.036]	0.657 [0.295, 1.464]	0.420 [0.187, 0.942]
(N = 67)	0.006*	0.075	0.304	0.035*
Left Occipital	0.592 [0.438, 0.801]	1.027 [0.994, 1.061]	2.003 [0.704, 5.702]	0.950 [0.560, 1.611]
(N = 45)	< 0.001**	0.105	0.193	0.850
Left Parietal	0.722 [0.562, 0.928]	1.019 [0.992, 1.046]	0.515 [0.222, 1.195]	0.388 [0.172, 0.874]
(N = 67)	0.011*	0.168	0.122	0.022*
Left Temporal	0.787 [0.639, 0.979]	1.034 [1.010, 1.059]	1.921 [0.671, 5.500]	0.255 [0.072, 0.896]
(N = 73)	0.031*	0.005*	0.224	0.033*
Right Central	0.562 [0.403, 0.784]	1.036 [0.988, 1.086]	0.762 [0.247, 2.346]	0.451 [0.143, 1.427]
(N = 33)	< 0.001**	0.145	0.635	0.176
Right Frontal	0.646 [0.460, 0.906]	1.046 [1.016, 1.076]	0.870 [0.307, 2.466]	0.424 [0.176, 1.025]
(N = 48)	0.011*	0.003*	0.793	0.057

FA = fractional anisotropy, M = male as the reference; EOR = extend of resection, gross total resection (GTR) > 90% as the reference. *Statistically significant for $p < 0.05$; **Statistically significant for $p < 0.001$.

Tumor Loc.	FA	Age	Gender (M)	EOR (> 90%)
Right Occipital	0.563 [0.376, 0.842]	1.023 [0.981, 1.067]	0.327 [0.070, 1.536]	0.469 [0.105, 2.102]
(N = 32)	0.005*	0.281	0.157	0.323
Right Parietal	0.753 [0.580, 0.977]	1.055 [1.012, 1.100]	0.426 [0.141, 1.289]	0.632 [0.231, 1.727]
(N = 43)	0.033*	0.011*	0.131	0.371
Right Temporal	0.926 [0.858, 0.982]	1.024 [1.002, 1.047]	1.699 [0.669, 4.313]	0.762 [0.247, 2.346]
(N = 62)	0.151	0.031*	0.265	0.635

FA = fractional anisotropy, M = male as the reference; EOR = extend of resection, gross total resection (GTR) > 90% as the reference. *Statistically significant for $p < 0.05$; **Statistically significant for $p < 0.001$.

Sex showed inconsistent associations with survival across models, none of which reached statistical significance. Higher EOR consistently favored improved survival but did not reach statistical significance (Table 3). These results were consistent when analyses were stratified by tumor location within cerebral lobes. Notably, normal FA values in the white matter structures reconstructed via correlational fiber tracking were significantly associated (*p* values ranging between 0.033 and < 0.001) with longer survival, with HRs ranging from 0.461 to 0.787. The temporal lobe was an exception, showing a non-significant association ($p = 0.151$; HR = 0.926, 95% CI: 0.858–0.982). Further details are available in Table 3.

Correlations

OS showed a significant linear correlation ($p < 0.001$) with mean FA values in the reconstructed fiber tracts for tumors across the whole brain ($r = 0.306$), as well as for left-hemispheric ($r = 0.304$) and right-hemispheric glioblastomas ($r = 0.324$; **Supplementary Results**, **Table S3**). However, correlation coefficients derived from exponential models were significantly higher for tumors distributed throughout the brain ($r = 0.356$; AIC difference = 2144), the left hemisphere ($r = 0.339$; AIC difference = 1141), and the right hemisphere ($r = 0.371$; AIC difference = 847; **Supplementary Results**, **Table S3** and Fig. 5). This tendency toward higher correlations in exponential models was also evident for tumor locations within individual cerebral lobes (**Supplementary Results**, **Table S3**). The exponential models provided a superior fit to the data compared to the linear model, with an AIC difference > 10 (range, 82–261) with the exception of left-centrally located tumors, where an AIC difference of 4 indicates only a moderate superiority of the exponential model. Notably, the strongest correlation coefficients were found in brain lobes that also exhibited the most significant log-rank results in the Kaplan-Meier survival analysis, namely the left frontal lobe, right central region, and right occipital lobe (see also Table 2).

Discussion

This study demonstrates that mesoscale connectomics, implemented through connectometry and correlational tractography, can identify microstructural signatures within WM tracts that significantly correlate with OS in patients with glioblastoma. By quantifying subtle, spatially localized disruptions in WM integrity using FA values, we found a significant survival advantage in patients with unaffected fiber tract subcomponents, who exhibited approximately twice the mOS compared to those with affected structures. Conventional methods, such as calculation of mean FA values across entire fiber tracts or manual region-of-interest (ROI)-based approaches, had not yielded comparable results. However, previous DTI studies have demonstrated that reductions in peritumoral FA correspond to tumor cell infiltration and extracellular matrix degradation [29, 30]. Our study extended this concept by integrating mesoscale connectomics and clinical outcomes, linking local diffusion changes and global network integrity with prognosis of patients with glioblastoma.

Our findings highlight the projection system of the basal ganglia (particularly parts of the thalamic radiations) and the commissural pathways (especially parts of the corpus callosum) as key regions whose microstructural preservation most strongly correlates with improved OS. Moreover, the association between FA and OS was largely independent of tumor lateralization, although the effects were somewhat more pronounced in right-hemispheric tumors. These findings support our hypothesis that, in addition to established covariates such as EOR or age, the prognosis of glioblastoma patients is closely linked to the structural integrity of critical structures within the surrounding neural network.

The anterior and superior thalamic radiations serve as major conduits between cortical and subcortical regions and are essential for sensorimotor and cognitive integration [31]. Disruption of these tracts impairs communication across large-scale neural networks required for normal neurological function, thereby contributing to more pronounced clinical deficits and accelerated neurological decline [32]. The corpus callosum is a common route for transhemispheric tumor spread, and callosal infiltration is characteristic of so-called butterfly glioblastomas, which are associated with particularly poor prognosis [33]. The finding that higher FA values within corpus callosum subclusters corresponded to better outcomes is therefore consistent with the notion that disruption of interhemispheric connections exacerbates both functional impairment and tumor dissemination potential [34].

The observation that the intact integrity of specific tract subcomponents was associated with a significant improvement in patient survival holds potential implications for clinical practice. Kaplan-Meier and Cox regression analyses revealed that FA values within the normal range in survival-relevant tracts were associated with a significantly longer mOS (approximately twice the mOS) and hazard ratios of about 0.55 per 0.1 FA increment. These findings are consistent with previous, smaller studies reporting that lower peritumoral FA is associated with faster recurrence and reduced survival [35]. However, the present study extends these observations by demonstrating that these associations persist systematically across hemispheres and multiple lobar locations when examined within a local connectome-level framework. These results suggest that microstructural integrity of specific WM segments may represent sensitive imaging biomarkers of prognosis. The underlying mechanism likely involves GB cells preferentially migrating along WM fiber tracts, thereby inducing progressive tract

damage. From a practical perspective, incorporating tract-specific FA metrics into preoperative assessment could facilitate patient risk stratification and help to guide the prioritization of surgical or adjuvant treatment strategies. In addition, WM tract vulnerability may ultimately inform radiotherapy planning to minimize collateral radiation of high-priority fiber subclusters.

Several clinical studies have employed connectometry and correlational tractography to investigate associations between white matter tract integrity and clinical outcomes in neurological, behavioral, or neuropsychiatric conditions [16, 36]. These studies have identified tract segments whose diffusion metrics are statistically linked to disease severity, cognitive performance, or functional prognosis, complementing conventional tractography and supporting the development of more sensitive biomarkers for patient assessment and stratification. However, to date, only a few studies have applied this methodological approach to patients with gliomas.

Yang et al. investigated, in two separate studies [37, 38], the effect of O-6-methylguanine-DNA methyltransferase (MGMT) promoter methylation and 1p/19q co-deletion on structural connectivity alterations in patients with diffuse insular gliomas. Regarding MGMT status, the authors found that in left insular gliomas, the volume of affected inferior fronto-occipital fasciculus was positively correlated with methylation levels. In right insular gliomas, however, the anterior segment of the thalamic radiation and reticular tract exhibited a negative correlation with methylation levels. In patients with 1p/19q co-deletion, the anterior and superior thalamic radiations, fornix, and cingulum, had significant negative associations with co-deletion status. They concluded that these tracts are critical for maintaining the integrity of brain networks, and, regarding the thalamic radiations, their findings are consistent with our observations.

Meoded et al. [39] found that in children undergoing posterior fossa tumor resection, DTI connectometry revealed decreased connectivity in the corpus callosum, right corticothalamic, and right corticostriatal pathways in those who developed posterior fossa syndrome compared to children with intact language. Although survival data were not correlated, these findings underscore the critical role of these white matter tracts in functional outcomes.

Several studies have demonstrated that DTI-derived structural connectome features correlate significantly with OS in glioblastoma patients. Wei et al. [13] used DTI-based macroscale connectomics in two independent GBM cohorts (discovery n = 117, validation n = 42) and found that greater structural network disturbance, especially in distant normal-appearing brain regions, correlates with worse OS (HR = 1.46) and progression-free survival, while preserved connectivity and network reorganization are associated with better outcomes.

The study of Salvalaggio et al. [10] is another key study that linked DTI-derived macroscale connectome measures with OS in glioblastoma patients. The authors developed a white-matter tract density index (TDI) from preoperative tractography in two GB patient cohorts (discovery n = 112; replication n = 70). They found that TDI was significantly associated with OS and their predictive model outperformed traditional prognostic factors such as age, MGMT status, and EOR, emphasizing the critical role of

structural connectivity in determining patient outcomes. These findings support the utility of DTI macroscale connectomics as an advanced biomarker for survival prediction and patient stratification in glioblastoma. However, the approach of most previously published studies is a global network analysis and not a mesoscale connectome analysis as in our present study.

The regression analyses between FA and OS further underscore the predictive value of WM microstructure, showing significant linear and slightly stronger exponential correlations both globally and within hemispheric subgroups. The strongest correlations corresponded to lobes that also showed the most significant log-rank results in Kaplan-Meier analyses, specifically the left frontal lobe, right central region, and right occipital lobe, highlighting the robustness of WM integrity in select tracts as a critical determinant of OS. The reason for the absence of a significant association in temporal lobe tumors remains unclear, as the present study was not specifically designed to investigate lobe-specific biological differences. Several factors may contribute, including subgroup size limitations, variability in tumor infiltration patterns, and differences in the anatomical organization and vulnerability of temporal white matter pathways. Further studies are required to investigate this issue. Notably, exponential modeling may capture non-linear effects of microstructural disruption on survival, suggesting a threshold effect wherein FA deterioration beyond a critical level leads to rapid clinical decline. Similar patterns have been observed in neurodegenerative diseases, such as Alzheimer's and amyotrophic lateral sclerosis, where progressive WM disintegration accelerates functional loss once structural connectivity falls below critical network tolerances [40, 41].

Despite these encouraging findings, several limitations of this study warrant consideration. The retrospective design and reliance on publicly available imaging databases limit control over acquisition parameters, treatment regimens, molecular subtype and clinical follow-up information.

First, although the DTI protocol adheres to clinical standards, it inherently involves trade-offs among spatial and angular resolution, the number of b-values, and acquisition time to remain compatible with clinical workflows. Given the low angular resolution and the use of a single b-value, the application of generalized q-sampling imaging (GQI) was not feasible under these conditions [21]. GQI generally achieves superior resolution of crossing fibers. However, accurate results typically require more than 30 unique diffusion directions and additional b-values exceeding 1000 s/mm² for optimal performance. Therefore, we chose to evaluate DTI-based FA values. While FA is a sensitive marker of microstructural integrity, it lacks specificity to particular tissue alterations. FA alterations may partly reflect the combined effects of tumor infiltration, edema, demyelination, secondary degeneration and/or disruption of vulnerable white matter networks. Future studies integrating quantitative tumor burden, complementary metrics like radial and axial diffusivity, and molecular/radiological characteristics from multi-modal MRI are required to determine the incremental prognostic value of connectomic markers and for additional insights into tract damage. Furthermore, DTI is limited in regions of complex fiber geometry, such as crossing or branching fibers [42]. Future studies using advanced diffusion models, such as high angular resolution diffusion imaging (HARDI) [43] or q-space imaging (QSI) [44], could refine tract-specific metrics and better distinguish tumor infiltration from vasogenic edema. However, assembling a

comparably large glioblastoma dataset poses a major challenge due to the long acquisition times required by these advanced techniques, necessitating coordinated collaboration across multiple specialized centers.

Second, no information regarding the postoperative treatment regimen implemented for each patient was available and could therefore not be taken into account. However, treatment management, particularly following the almost inevitable occurrence of recurrence, is a critical determinant of patient survival [45]. It should also be noted that modern therapeutic strategies for glioblastoma recurrences, especially for multiple relapses, are highly individualized, leading to complex treatment courses that are difficult to capture comprehensively in survival analyses [46]. Nonetheless, future studies should consider incorporating a simplified scheme to account for these treatment variations.

Third, the integration of molecular characteristics of glioblastomas (e.g., MGMT promoter methylation, EGFR amplification) and patient condition metrics (e.g., Karnofsky Performance Status, KPS) was not possible due to unavailability or significant incompleteness of this information. These variables represent important covariates and should be incorporated into the analyses of future studies.

Fourth, our analyses did not include area under the receiver operating characteristic curve (AUROC) evaluation or other comprehensive predictive performance metrics, which would have strengthened the evidence for the prognostic utility of the identified white matter tracts. However, the primary aim of the present study was exploratory and mechanistic, namely to identify survival-associated white matter substructures using correlational tractography and connectometry. Furthermore, a recently published study [47] integrated a more fine-grained graph-theoretical structural connectome metrics derived from glioblastoma patients into machine-learning survival models and performed extensive predictive performance evaluations, demonstrating strong performance for overall survival (OS) prediction. Finally, longitudinal imaging was not available in this dataset, limiting the ability to assess temporal changes in tract integrity and their relationship to treatment response, tumor progression, or recurrence localization. Prospective longitudinal imaging could help determine whether FA decline precedes clinical or radiological progression and distinguish tumor infiltration from secondary degeneration, thereby positioning connectometry as a potential predictive biomarker rather than merely a correlative one.

In conclusion, this study provides strong evidence that microstructural integrity of specific WM subcomponents, as identified through connectometry and correlational tractography, serves as a significant predictor of OS in glioblastoma patients. The findings support the emerging paradigm that glioblastomas should be understood as a network-level disease, with outcomes influenced not only by focal tumor burden but also by the preservation of structural connectivity. The strongest associations observed within projection and commissural tracts underscore the essential role of large-scale integration pathways in maintaining neurological function and survival. While future prospective multicenter validation studies with harmonized diffusion acquisition protocols, independent external cohorts, and longitudinal designs remain essential before clinical implementation, these findings

highlight the promise of mesoscale connectomics as a powerful tool for advancing our understanding of glioblastoma biology and improving patient care.

Declarations

Author Contribution

Conceptualization: A.S. and S.O.; methodology: A.S., U.M-B., and A.M-B.; software: A.S.; formal analysis: A.S.; investigation: A.S., M.D.; validation: A.S., G.H., F.M. and S.O.; resources: G.H. and O.S.; data curation: A.S. and A.M-B.; writing—original draft preparation: A.S.; writing, review, and editing: A.S., S.O., G.H., A.D., F.M., O.S., M.D., U.M-B., A.M-B.; visualization: A.S.; supervision: S.O., G.H., A.D., F.M., and O.S.; project administration: A.S.; funding acquisition: A.S. All authors have read and agreed to the published version of the manuscript.

References

1. Angom RS, Nakka NMR, Bhattacharya S (2023) Advances in Glioblastoma Therapy: An Update on Current Approaches. Brain Sci 13:1536. https://doi.org/10.3390/brainsci13111536
2. Poon MTC, Sudlow CLM, Figueroa JD, Brennan PM (2020) Longer-term (≥ 2 years) survival in patients with glioblastoma in population-based studies pre- and post-2005: a systematic review and meta-analysis. Sci Rep 10:11622. https://doi.org/10.1038/s41598-020-68011-4
3. Li YM, Suki D, Hess K, Sawaya R (2016) The influence of maximum safe resection of glioblastoma on survival in 1229 patients: Can we do better than gross-total resection? J Neurosurg 124:977–988. https://doi.org/10.3171/2015.5.JNS142087
4. Sun Y, Wang X, Zhang DY et al (2025) Brain-wide neuronal circuit connectome of human glioblastoma. Nature 641:222–231. https://doi.org/10.1038/s41586-025-08634-7
5. Tetzlaff SK, Reyhan E, Layer N et al (2025) Characterizing and targeting glioblastoma neuron-tumor networks with retrograde tracing. Cell 188:390–411e36. https://doi.org/10.1016/j.cell.2024.11.002
6. Jang K, Back M (2025) Spatial Mapping of Glioblastoma Infiltration: Diffusion Tensor Imaging-Based Radiomics and Connectomics in Recurrence Prediction. Brain Sci 15:576. https://doi.org/10.3390/brainsci15060576
7. Seker-Polat F, Pinarbasi Degirmenci N, Solaroglu I, Bagci-Onder T (2022) Tumor Cell Infiltration into the Brain in Glioblastoma: From Mechanisms to Clinical Perspectives. Cancers (Basel) 14:443. https://doi.org/10.3390/cancers14020443
8. Hazaymeh M, Löber-Handwerker R, Döring K et al (2022) Prognostic differences and implications on treatment strategies between butterfly glioblastoma and glioblastoma with unilateral corpus callosum infiltration. Sci Rep 12:19208. https://doi.org/10.1038/s41598-022-23794-6
9. Behrens TE, Sporns O (2012) Human connectomics. Curr Opin Neurobiol 22:144–153. https://doi.org/10.1016/j.conb.2011.08.005

10. Salvalaggio A, Pini L, Bertoldo A, Corbetta M (2024) Glioblastoma and brain connectivity: the need for a paradigm shift. Lancet Neurol 23:740–748. https://doi.org/10.1016/S1474-4422(24)00160-1
11. Krishna S, Choudhury A, Keough MB et al (2023) Glioblastoma remodelling of human neural circuits decreases survival. Nature 617:599–607. https://doi.org/10.1038/s41586-023-06036-1
12. Kennedy H, Van Essen DC, Christen Y (2016) Micro-, Meso- and Macro-Connectomics of the Brain. Springer International Publishing, Cham
13. Wei Y, Li C, Cui Z et al (2023) Structural connectome quantifies tumour invasion and predicts survival in glioblastoma patients. Brain 146:1714–1727. https://doi.org/10.1093/brain/awac360
14. Yeh F-C, Badre D, Verstynen T (2016) Connectometry: A statistical approach harnessing the analytical potential of the local connectome. NeuroImage 125:162–171. https://doi.org/10.1016/j.neuroimage.2015.10.053
15. Yeh F-C, Irimia A, Bastos DC, de Golby A AJ (2021) Tractography methods and findings in brain tumors and traumatic brain injury. NeuroImage 245:118651. https://doi.org/10.1016/j.neuroimage.2021.118651
16. Li M-J, Yeh F-C, Huang S-H et al (2022) Differential Tractography and Correlation Tractography Findings on Patients With Mild Traumatic Brain Injury: A Pilot Study. Front Hum Neurosci 16. https://doi.org/10.3389/fnhum.2022.751902
17. Bakas S, Sako C, Akbari H et al (2022) The University of Pennsylvania glioblastoma (UPenn-GBM) cohort: advanced MRI, clinical, genomics, & radiomics. Sci Data 9:453. https://doi.org/10.1038/s41597-022-01560-7
18. Yeh F-C (2025) DSI Studio: an integrated tractography platform and fiber data hub for accelerating brain research. Nat Methods 22:1617–1619. https://doi.org/10.1038/s41592-025-02762-8
19. Yeh F-C, Wedeen VJ, Tseng W-YI (2011) Estimation of fiber orientation and spin density distribution by diffusion deconvolution. NeuroImage 55:1054–1062. https://doi.org/10.1016/j.neuroimage.2010.11.087
20. Yeh F-C, Vettel JM, Singh A et al (2016) Quantifying Differences and Similarities in Whole-Brain White Matter Architecture Using Local Connectome Fingerprints. PLOS Comput Biol 12:e1005203. https://doi.org/10.1371/journal.pcbi.1005203
21. Yeh F-C, Wedeen VJ, Tseng W-YI (2010) Generalized q-Sampling Imaging. IEEE Trans Med Imaging 29:1626–1635. https://doi.org/10.1109/TMI.2010.2045126
22. Yeh F-C, Panesar S, Fernandes D et al (2018) Population-averaged atlas of the macroscale human structural connectome and its network topology. NeuroImage 178:57–68. https://doi.org/10.1016/j.neuroimage.2018.05.027
23. Yeh F-C, Verstynen TD, Wang Y et al (2013) Deterministic Diffusion Fiber Tracking Improved by Quantitative Anisotropy. PLoS ONE 8:e80713. https://doi.org/10.1371/journal.pone.0080713
24. Yeh F-C, Panesar S, Barrios J et al (2019) Automatic Removal of False Connections in Diffusion MRI Tractography Using Topology-Informed Pruning (TIP). Neurotherapeutics 16:52–58. https://doi.org/10.1007/s13311-018-0663-y

25. JASP Team (2025) JASP
26. R Core Team (2021) R: A language and environment for statistical computing
27. Kaplan EL, Meier P (1958) Nonparametric Estimation from Incomplete Observations. J Am Stat Assoc 53:457. https://doi.org/10.2307/2281868
28. Lin H, Zelterman D (2002) Modeling Survival Data: Extending the Cox Model. Technometrics 44:85–86. https://doi.org/10.1198/tech.2002.s656
29. Stadlbauer A, Ganslandt O, Buslei R et al (2006) Gliomas: Histopathologic Evaluation of Changes in Directionality and Magnitude of Water Diffusion at Diffusion-Tensor MR Imaging. Radiology 240:803–810. https://doi.org/10.1148/radiol.2403050937
30. Lu S, Ahn D, Johnson G et al (2004) Diffusion-Tensor MR Imaging of Intracranial Neoplasia and Associated Peritumoral Edema: Introduction of the Tumor Infiltration Index. Radiology 232:221–228. https://doi.org/10.1148/radiol.2321030653
31. Jitsuishi T, Yamaguchi A (2025) Structural connector hub properties of the thalamus in large-scale brain networks: white matter structure as an anatomical basis. NeuroImage 317:121333. https://doi.org/10.1016/j.neuroimage.2025.121333
32. Li S, Gao L, Liu Y et al (2019) Unilateral thalamic glioma disrupts large-scale functional architecture of human brain during resting state. Neuropsychiatr Dis Treat Volume 15:947–956. https://doi.org/10.2147/NDT.S186161
33. Bjorland LS, Dæhli Kurz K, Fluge Ø et al (2022) Butterfly glioblastoma: Clinical characteristics, treatment strategies and outcomes in a population-based cohort. Neuro-Oncology Adv 4. https://doi.org/10.1093/noajnl/vdac102
34. Palmisciano P, Ferini G, Watanabe G et al (2022) Gliomas Infiltrating the Corpus Callosum: A Systematic Review of the Literature. Cancers (Basel) 14:2507. https://doi.org/10.3390/cancers14102507
35. Jin Y, Randall JW, Elhalawani H et al (2020) Detection of Glioblastoma Subclinical Recurrence Using Serial Diffusion Tensor Imaging. Cancers (Basel) 12:568. https://doi.org/10.3390/cancers12030568
36. Yeh F-C, Tang P-F, Tseng W-YI (2013) Diffusion MRI connectometry automatically reveals affected fiber pathways in individuals with chronic stroke. NeuroImage Clin 2:912–921. https://doi.org/10.1016/j.nicl.2013.06.014
37. Yang Z, Xue B, Song X et al (2024) Connectomic insights into the impact of 1p/19q co-deletion in dominant hemisphere insular glioma patients. Front Neurosci 18. https://doi.org/10.3389/fnins.2024.1283518
38. Yang Z, Yin C, Yeh F et al (2024) Exploring MGMT methylation-driven structural connectivity changes in insular gliomas: a tractography and graph theoretical analysis. J Neurooncol 166:155–165. https://doi.org/10.1007/s11060-023-04539-5
39. Meoded A, Jacobson L, Liu A et al (2020) Diffusion Tensor Imaging Connectomics Reveals Preoperative Neural Connectivity Changes in Children with Postsurgical Posterior Fossa Syndrome. J Neuroimaging 30:192–197. https://doi.org/10.1111/jon.12686

40. Li W, Wei Q, Hou Y et al (2021) Disruption of the white matter structural network and its correlation with baseline progression rate in patients with sporadic amyotrophic lateral sclerosis. Transl Neurodegener 10:35. https://doi.org/10.1186/s40035-021-00255-0
41. Phillips JS, Adluru N, Chung MK et al (2024) Greater white matter degeneration and lower structural connectivity in non-amnestic vs. amnestic Alzheimer's disease. Front Neurosci 18. https://doi.org/10.3389/fnins.2024.1353306
42. Suo X, Guo L, Fu D et al (2021) A Comparative Study of Diffusion Fiber Reconstruction Models for Pyramidal Tract Branches. Front Neurosci 15. https://doi.org/10.3389/fnins.2021.777377
43. Tuch DS, Reese TG, Wiegell MR et al (2002) High angular resolution diffusion imaging reveals intravoxel white matter fiber heterogeneity. Magn Reson Med 48:577–582. https://doi.org/10.1002/mrm.10268
44. Van AT, Granziera C, Bammer R (2010) An Introduction to Model-Independent Diffusion Magnetic Resonance Imaging. Top Magn Reson Imaging 21:339–354. https://doi.org/10.1097/RMR.0b013e31823e6303
45. Anwer MS, Abdel-Rasol MA, El-Sayed WM (2025) Emerging therapeutic strategies in glioblastsoma: drug repurposing, mechanisms of resistance, precision medicine, and technological innovations. Clin Exp Med 25:117. https://doi.org/10.1007/s10238-025-01631-0
46. Singh S, Dey D, Barik D et al (2025) Glioblastoma at the crossroads: current understanding and future therapeutic horizons. Signal Transduct Target Ther 10:213. https://doi.org/10.1038/s41392-025-02299-4
47. Stadlbauer A, Oberndorfer S, Heinz G et al (2026) Machine-Learning-Based Survival Prediction in Glioblastoma Using Graph-Theoretical Analysis of Structural Network Alterations. Cancers (Basel) 18:1161. https://doi.org/10.3390/cancers18071161

Figures

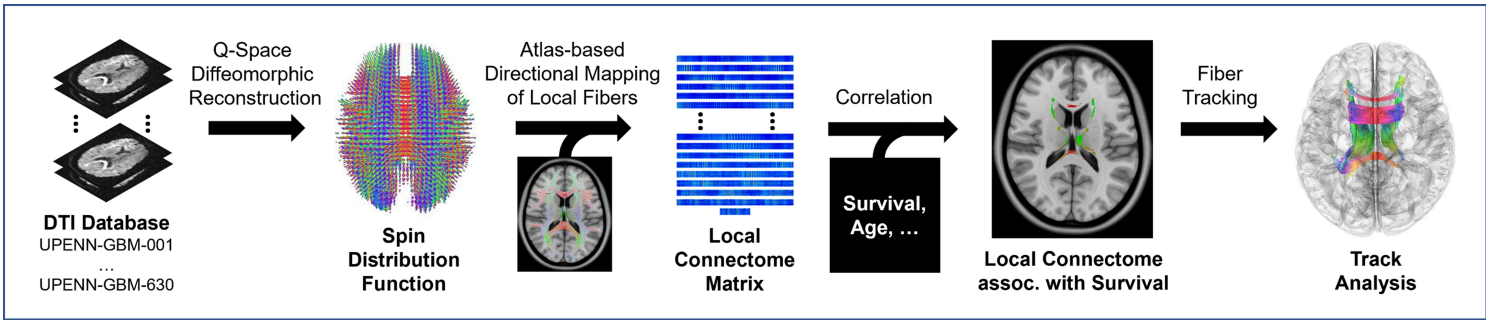


Figure 1

Flowchart of connectometry and correlational tractography analysis. The first step is the transformation of DTI data into a standardized format using q-space diffeomorphic reconstruction (QSDR). Additionally, the spin distribution function (SDF) is employed to determine the quantity or concentration of water

diffusion in different orientations within a particular voxel. The SDF are sampled and structured into a local connectome matrix. The term “local connectome” refers to the degree of connectivity between adjacent voxels within a white matter fascicle, defined by the density of diffusing spins. The association of this matrix with overall survival is adjusted for factors like age, gender, and extend of resection ultimately leading to the identification of fiber components with significant correlations.

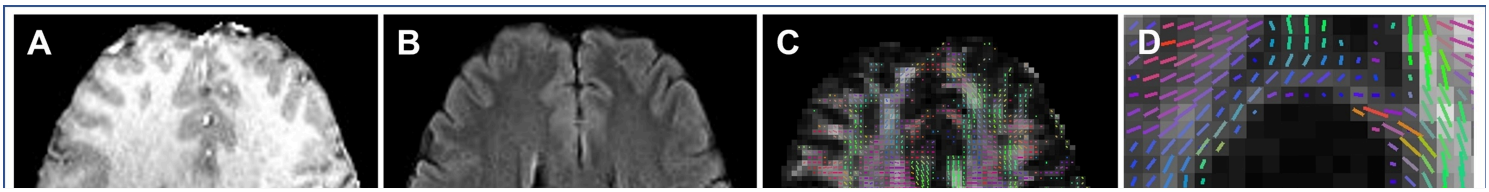


Figure 2

Illustrative case for calculation of the spin distribution function (SDF). Preoperative MR images including contrast-enhanced (CE) T1-weighted (**A**), FLAIR MRI (**B**) and FA map from DTI data overlayed with the SDF information (**C**) for a 43-year-old male patient with an overall survival of 2838 days (ID: UPENN-GBM-00003). **D**, shows an enlarged section of C corresponding to the white frame.

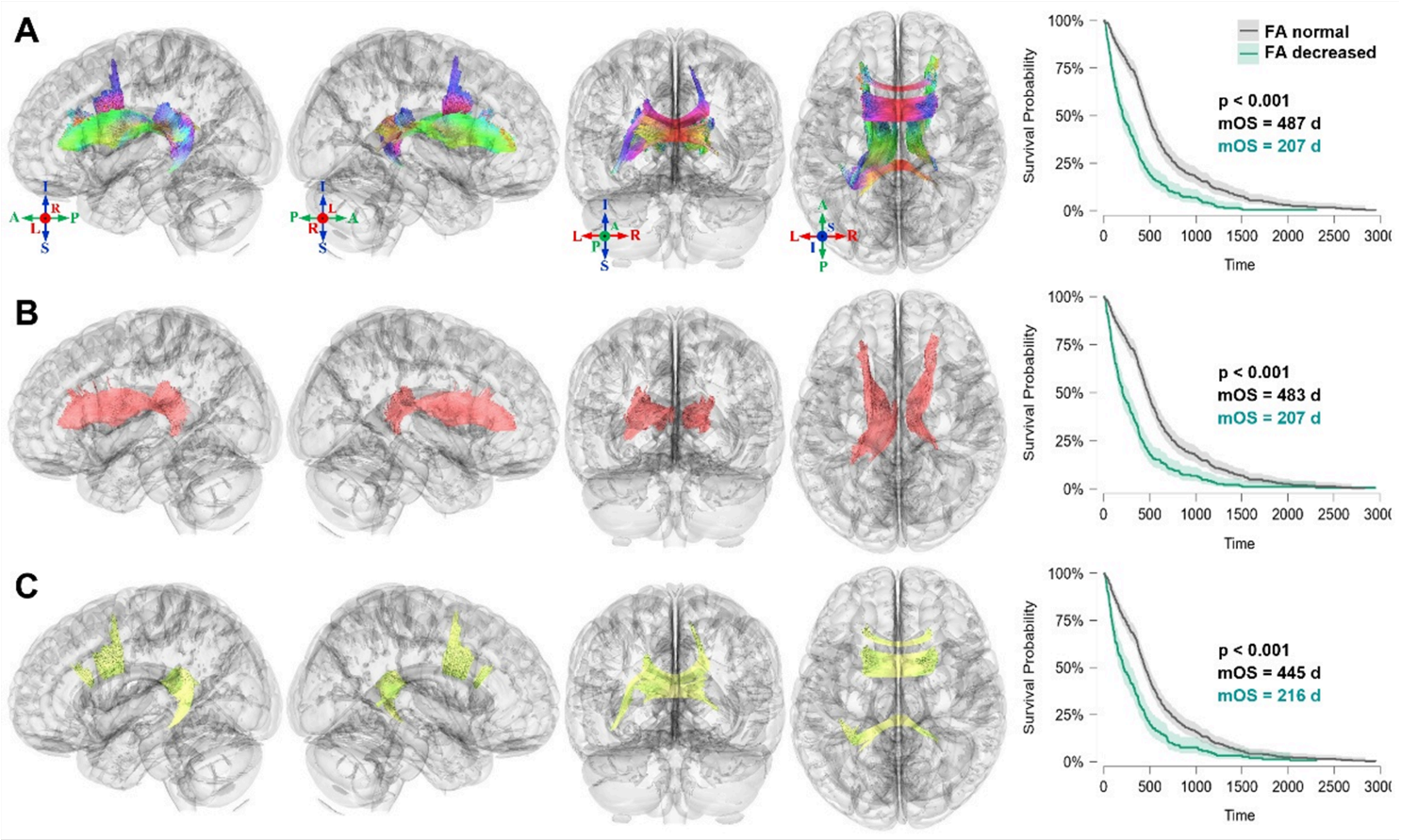


Figure 3

Correlational tractography of glioblastomas located throughout the brain. **A**, Reconstructed fiber segments exhibiting a significant positive correlation with overall survival (OS). The tractogram is color-coded according to fiber orientation, as indicated by the coordinate axes in the lower left corner (A = anterior, P = posterior, I = inferior, S = superior, L = left, R = right). The panel on the far right displays Kaplan–Meier survival curves for normal FA values (gray) and reduced FA values (green) within these fiber segments. The median OS (mOS) values and the log-rank test p-values are shown in the diagrams (d = days). **B**, Tractogram showing the subclusters of basal ganglia projection tracts (red), extracted via tract recognition from the tractogram presented in Figure subpart A. The corresponding Kaplan–Meier survival curves are shown on the far right. **C**, Tractogram of corpus callosum subclusters (yellow) extracted using tract recognition, along with the corresponding Kaplan–Meier survival curves.

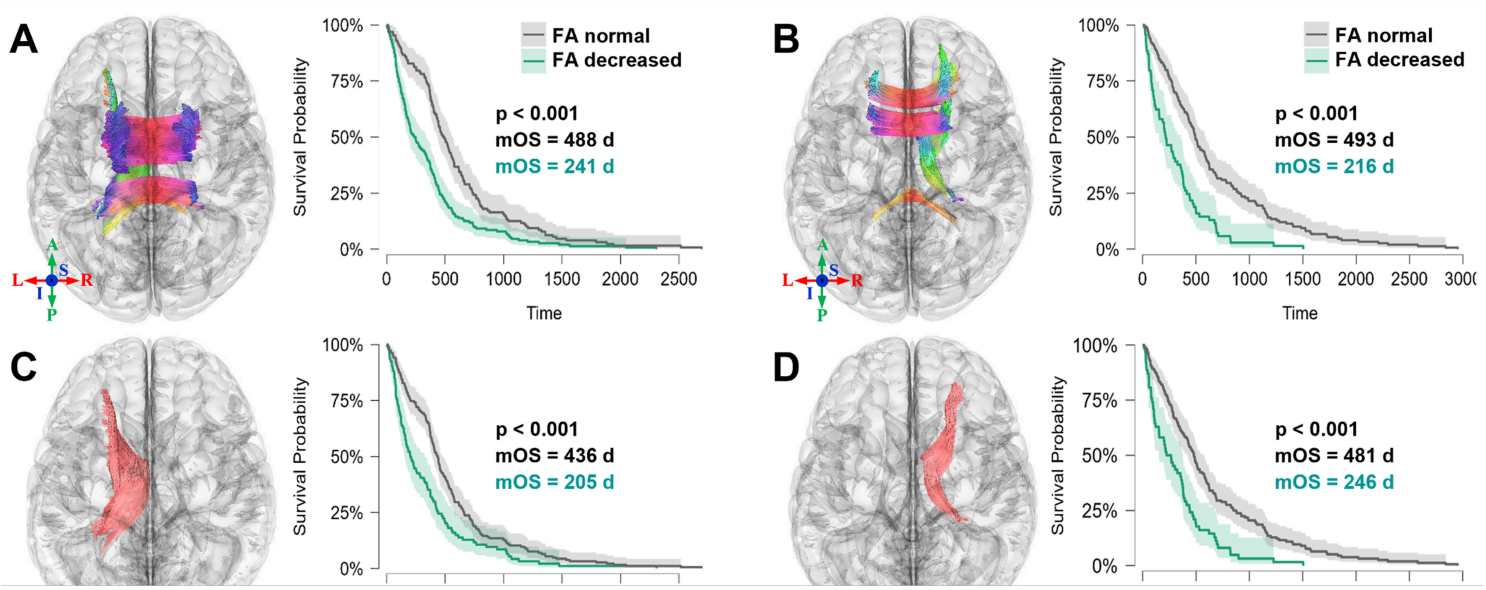


Figure 4

Correlational tractography of left- and right-hemispheric glioblastomas. **A**, Reconstructed fiber segments exhibiting a significant positive correlation with overall survival (OS) in patients with left-hemispheric tumors. The tractogram is color-coded according to fiber orientation, as indicated by the coordinate axes in the lower left corner (A = anterior, P = posterior, I = inferior, S = superior, L = left, R = right). The panel on the right displays Kaplan–Meier survival curves for normal FA values (gray) and reduced FA values (green) within these fiber segments. The median OS (mOS) values and the log-rank test p-values are shown in the diagrams (d = days). **B**, Reconstructed fiber segments showing a significant positive correlation with OS, along with corresponding Kaplan–Meier survival curves, for patients with right-hemispheric tumors. **C** and **D**, Tractograms of basal ganglia projection tract subclusters (red) for left- and right-hemispheric glioblastomas, respectively, extracted using tract recognition from the tractogram presented in Figure subparts A and B. The corresponding Kaplan–Meier survival curves are shown on the right. **E** and **F**, Tractogram of corpus callosum subclusters (yellow) for left- and right-hemispheric glioblastomas, respectively, extracted using tract recognition, along with the corresponding Kaplan–Meier survival curves.

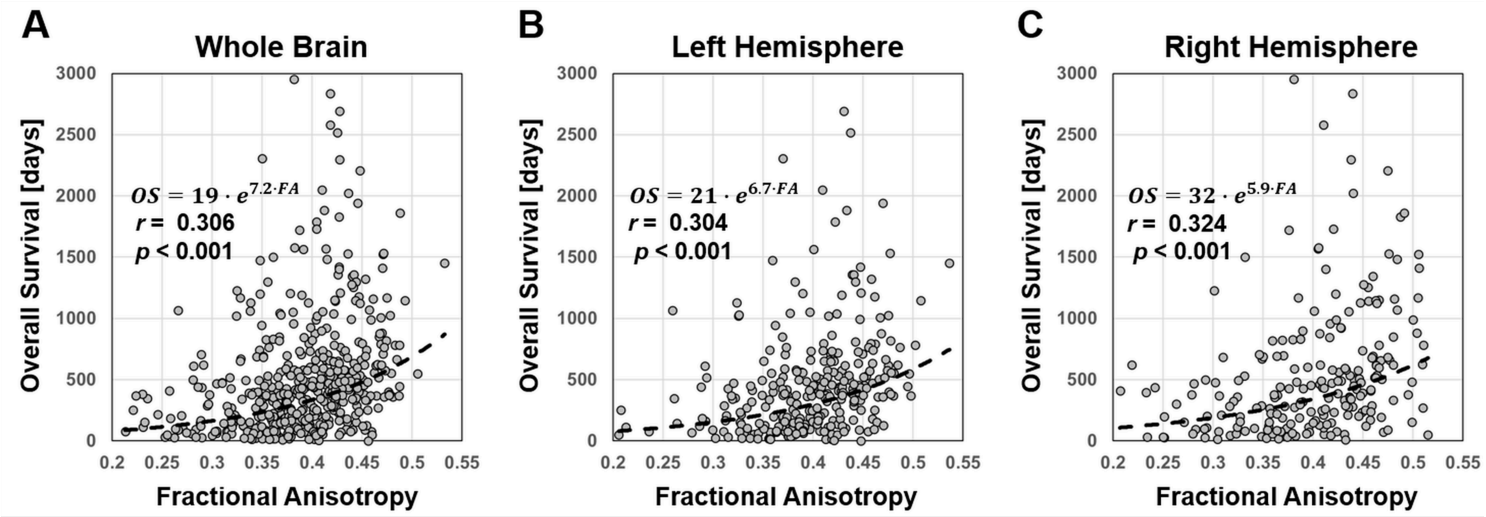


Figure 5

Scatterplots of the relationship between overall survival (OS) and fractional anisotropy (FA). **A**, Exponential regression analysis between OS and FA values averaged across the reconstructed fiber segments in patients with tumor locations distributed throughout the brain, as shown in Figures 1A. **B** and **C**, Exponential regression analysis between OS and FA values averaged across the reconstructed fiber segments for left- and right-hemispheric glioblastomas, respectively, as shown in Figures 2A and 2B.

Supplementary Files

This is a list of supplementary files associated with this preprint. Click to download.

- SupplementaryMaterials.pdf